CWP-669

Estimation of interval shear-wave attenuation from mode-converted data

Bharath Shekar & Ilya Tsvankin

ABSTRACT

Interval attenuation measurements provide valuable information for reservoir characterization and lithology discrimination. Here, we extend the attenuation layer-stripping method of Behura and Tsvankin to mode-converted (PS) waves with the goal of estimating the interval S-wave attenuation coefficient. By identifying PP and PS events with shared ray segments and applying the PP+PS=SS method, we first perform kinematic construction of pure shear (SS) events in the target layer and overburden. Then, the modified spectral-ratio method is used to compute the effective shear-wave attenuation coefficient for the target reflection. Finally, application of the dynamic version of velocity-independent layer stripping to the constructed SS reflections yields the interval S-wave attenuation coefficient in the target layer. The attenuation coefficient estimated for a range of source-receiver offsets can be inverted for the interval attenuation-anisotropy parameters. The method is tested on a multicomponent synthetic data set from layered VTI (transversely isotropic with a vertical symmetry axis) media generated with the anisotropic reflectivity method.

Key words: attenuation, anisotropy, multicomponent data, shear waves

Introduction

Attenuation analysis provides seismic attributes sensitive to the physical properties of the subsurface. Reliable attenuation measurements have become feasible with acquisition of high-quality reflection and borehole data. Attenuation is often found to be anisotropic (directionally dependent) due to a variety of factors such as the intrinsic anisotropy of the material, the presence of aligned fluid-fractures (Batzle et al., 2005), or interbedding of thin layers with different properties (Zhu et al., 2007). The magnitude of attenuation anisotropy can be much higher than that of velocity anisotropy, and the symmetry of the attenuation coefficient can be different than that of the velocity function (Liu et al., 2007).

The quality factors Q_P and Q_S are widely used as measures of P- and S-wave intrinsic attenuation, respectively (Zhu, 2006). Dvorkin and Mavko (2006) observe that the ratio Q_S^{-1}/Q_P^{-1} can serve as an indicator of hydrocarbons because the values of Q_P and Q_S in fluid-saturated rocks are close, while in dry or gas-saturated rocks $Q_P \gg Q_S$. Adam (2008) suggests that time-lapse studies of attenuation are useful in monitoring reservoir fluids. Chichinina et al. (2009) conduct ultrasonic laboratory experiments for models with VTI symmetry. Their results show that the symmetry-axis attenuation of P-waves is much greater than that of S-waves in dry samples, while for oil-saturated models, the two models have comparable attenuation. Shear-wave attenuation in heavy oils is closely linked to temperature, and hence could be useful in seismic monitoring of thermal recovery processes (Behura et al., 2007).

De et al. (1994) report measurements of the shear-wave quality factor from vertical seismic profiling (VSP) surveys and sonic logs. It is more difficult to study S-wave attenuation using reflection data due to such problems as the high level of noise and statics problems for shear waves. Behura and Tsvankin (2009) combine the velocity-independent layer stripping (VILS) method of Dewangan and Tsvankin (2006) with the spectral-ratio method to estimate the interval attenuation of pure PP or SS reflected waves. They identify the overburden and target events that share ray segments in the overburden to compute the interval traveltime and then the interval attenuation coefficient in the target layer. Their algo-

rithm is data-driven and does not require information about the velocity or attenuation in the overburden.

Shear waves, however, cannot be excited offshore, and shear-wave sources are seldom used on land. Therefore, here we extend the technique of Behura and Tsvankin (2009) to mode-converted data by supplementing it with the PP+PS=SS method of Grechka and Tsvankin (2002). First, we discuss how the PP+PS=SS method can be combined with VILS to construct SS-wave moveout in the target layer and overburden from PP and PS data. Then the interval S-wave attenuation coefficient is obtained by extending the kimenatic construction procedure to frequency-domain amplitudes processed using the spectral-ratio method. Finally, we apply the algorithm to synthetic data generated for a layered VTI medium and investigate the accuracy of the inversion for the SV-wave attenuation-anisotropy parameters.

Methodology

For simplicity, the method is described for 2D models, but it can be extended to 3D wide-azimuth data. We operate with pure-mode (PP) and mode-converted (PS) reflections for a medium with an arbitrarily anisotropic, heterogeneous target layer overlaid by a laterally homogeneous overburden with a horizontal symmetry plane in each layer. In the 2D version of the method the vertical incidence plane is supposed to be a plane of mirror symmetry for the whole model. Therefore, both rays and the corresponding phase-velocity vectors are confined to the incidence plane, and converted waves represent in-plane polarized PSV modes. The P-to-S conversion is assumed to occur only at the reflector. We begin with a description of the algorithm designed to compute the interval shear-wave traveltimes and then discuss estimation of the interval shear-wave attenuation coefficient in the target layer.

Kinematic layer stripping for interval shear-wave traveltimes

To estimate the interval shear-wave traveltimes in the target layer, we combine the PP+PS=SS method with velocity-independent layer stripping (VILS) developed by Dewangan and Tsvankin (2006). Suppose P-wave sources and receivers of both P- and S-waves are continuously distributed along the acquisition line. As discussed by Grechka and Tsvankin (2002), matching time slopes on common-receiver gathers at the source location A allows us to identify the PP (ARB) and PS (ARC) target events that share the downgoing segment AR and the reflection point R at the bottom of the target layer (Figure 1). Likewise, for a P-wave source at B, we find PP (BRA) and PS (BRD) target events that share the downgoing segment BR. This procedure

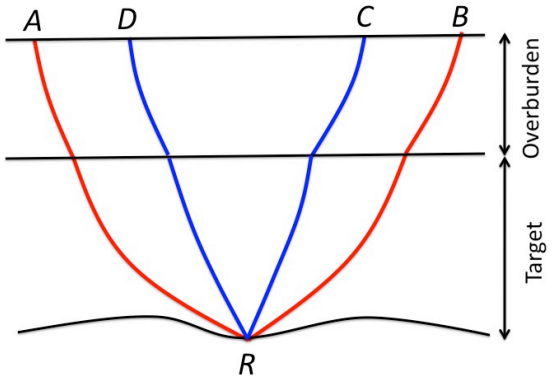

Figure 1. 2D ray diagram illustrating the PP+PS=SS method for PP and PS reflections from the bottom of the target layer. The wavefield is excited in split-spread geometry by P-wave sources located at points A and B. Target PP (ARB) and PS (ARC) events share the downgoing segment AR and, therefore the reflection point R at the bottom of the target layer. Another pair of PP (BRA) and PS (BRD) target events share the downgoing segment BR. The constructed SS target event corresponds to DRC.

makes it possible to construct the SS event DRC, where C and D are the coordinates of S-wave receivers. For brevity, we denote the PP (ARB) and PS (ARC and BRD) events by $\mathrm{PP_E}$, $\mathrm{PS_{E1}}$, and $\mathrm{PS_{E2}}$ (respectively) and the constructed SS event DRC by $\mathrm{SS_E}$ ("E" refers to effective events reflected from the bottom of the target layer). The exact shear-wave traveltime for the reflection $\mathrm{SS_E}$ is (Grechka and Tsvankin, 2002)

$$t_{SS_E} = t_{PS_{E1}} + t_{PS_{E2}} - t_{PP_E}. \qquad (1)$$

The constructed event $\mathrm{SS_E}$ can be treated (in a kinematic sense) as a pure reflection mode excited by a shear-wave source.

Next, we find the interval shear-wave traveltime in the target layer, which requires knowledge of the traveltime in the overburden. Since the data are assumed to be generated with a P-wave source, it is necessary to apply the PP+PS=SS method repeatedly to construct SS reflections in the overburden (Figure 2). To layer-strip the segment DR of the SS-wave, we need to obtain the coordinate of point I and the traveltime along the overburden segment ID. Note that the horizontal slowness along any ray in the laterally homogeneous overburden should be preserved.

First, we form a common-receiver gather of the PS-wave at location D and identify the point (E) where the time slope (horizontal slowness) coincides with that at D. The obtained overburden PS event EID shares the segment ID with the target SS event CRD (Figure 2b). Then we form a common-source PP gather at location E to find the point F where the time slope (horizontal slowness) coincides with that at E, which means that

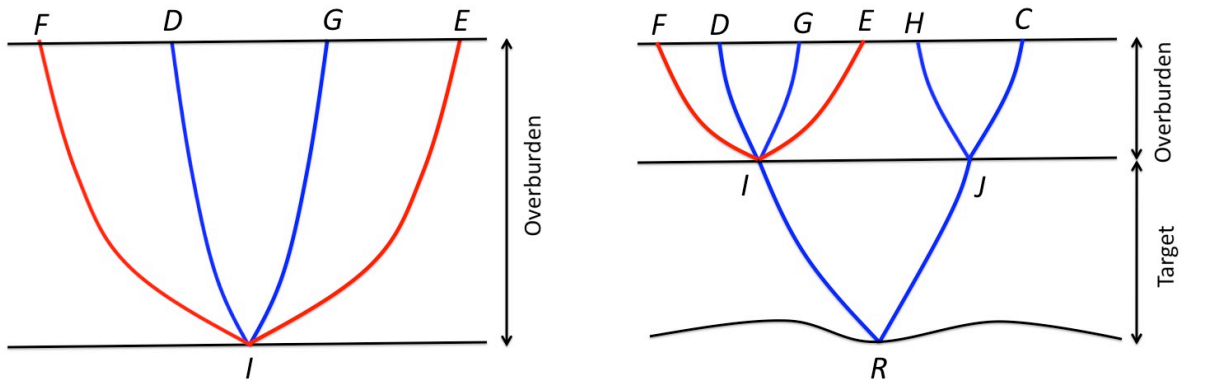

Figure 2. Layer stripping of the constructed SS events. (a) Application of the PP+PS=SS method is applied to kinematically construct pure SS-waves in the overburden. PP (EIF) and PS (EID) events share the downgoing segment EI and the reflection point I at the bottom of the overburden. Another pair of PP (FIE) and PS (FIG) overburden events share the downgoing segment FI. (b) The constructed overburden SS event DIG shares the segment ID with the target SS reflection.

the overburden PP event EIF shares the downgoing segment EI with the PS event EID (Figure 2a).

The moveout functions of the overburden PP, PS, and SS events are symmetric with respect to zero offset. Therefore, the receiver coordinate of the overburden PS event FIG can be found from

$$x_G = x_E + x_F - x_D. \tag{2}$$

The constructed event DIG (denoted by $\mathrm{SS}_{\mathrm{O1}}$, where "O" refers to the overburden and "1" to the left segment of the target SS event in Figure 2b) shares the segment ID with the target SS event DRC (Figure 2b). The PP event EIF will be denoted by $\mathrm{PP}_{\mathrm{O1}}$ and the PS events EID and FIG by $\mathrm{PS}_{\mathrm{O1}}$. The exact traveltime of the event $\mathrm{SS}_{\mathrm{O1}}$ is then given by

$$t_{SS_{O1}} = 2\,t_{PS_{O1}} - t_{PP_{O1}}, \tag{3}$$

and the lateral coordinate of location I is

$$x_I = \frac{x_D + x_G}{2}. \tag{4}$$

Likewise, we can apply the PP+PS=SS method to construct the overburden SS event HJC ($\mathrm{SS}_{\mathrm{O2}}$) that shares the segment JC with the target event SS_{E} (Figure 3). The corresponding traveltime $t_{SS_{O2}}$ and the lateral coordinate of point J are obtained using the algorithm discussed above. The interval shear-wave traveltime in the target layer is given by

$$t_{SS_T} = t_{SS_E} - \frac{1}{2}\left(t_{SS_{O1}} + t_{SS_{O2}}\right). \tag{5}$$

The interval traveltime t_{SS_T} corresponds to the raypath IRJ of the target event SS_{T}.

If the target is horizontal and laterally homogeneous, the raypaths of the downgoing and upgoing overburden events correspond to the same ray parameter and, therefore, are symmetric with respect to the vertical. Then $t_{SS_{O1}} = t_{SS_{O2}}$, and it is sufficient to apply the PP+PS=SS method just to one of the overburden segments of the target event SS_{E}.

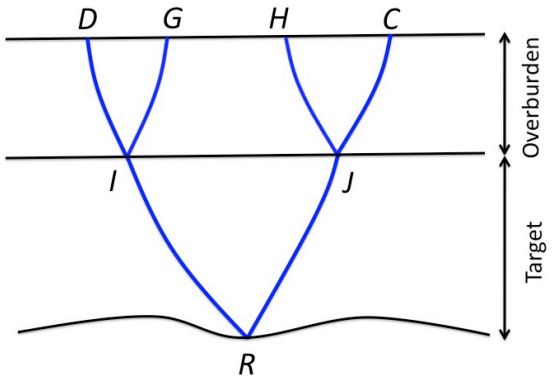

Figure 3. Raypaths of the constructed SS events. The target SS event DRC shares the segments ID and JC with the overburden events DIG and HJC, respectively. The method produces the interval traveltime along the raypath IRJ.

Layer stripping for interval shear-wave attenuation

Behura and Tsvankin (2009) combine VILS with the spectral-ratio method and apply their attenuation layer-stripping algorithm to frequency-domain amplitudes of pure-mode reflections. This technique can be extended to the combination of PP- and PS-waves analyzed

above. The ray-theoretic frequency-domain amplitudes of the waves $\mathrm{PP_E}$, $\mathrm{PS_{E1}}$ and $\mathrm{PS_{E2}}$ (Figure 1) can be written as

$$|U_{PP_E}| = S(\omega)\,\mathcal{G}_{PP_E}\; e^{-k^I_{P,AR}\,l_{AR}\,-\,k^I_{P,RB}\,l_{RB}}, \quad (6)$$

$$|U_{PS_{E1}}| = S(\omega)\,\mathcal{G}_{PS_{E1}}\; e^{-k^I_{P,AR}\,l_{AR}}\; e^{-k^I_{S,RC}\,l_{RC}}, \quad (7)$$

$$|U_{PS_{E2}}| = S(\omega)\,\mathcal{G}_{PS_{E2}}\; e^{-k^I_{P,BR}\,l_{BR}}\; e^{-k^I_{S,RD}\,l_{RD}}, \quad (8)$$

where $S(\omega)$ is the spectrum of the source wavelet. The coefficients $k^I_{P,XY}$ and $k^I_{S,XY}$ are the average P- and S-wave group attenuation coefficients along the raypath XY, the length of the raypath XY is denoted by l_{XY}. The coefficients $\mathcal{G}_{PP_E}$, $\mathcal{G}_{PS_{E1}}$ and $\mathcal{G}_{PS_{E2}}$ include the source/receiver directivity, reflection/transmission coefficients along the raypath, and the geometrical spreading of the corresponding events. Equations 6, 7, and 8 can be combined to compute the attenuation coefficient of the reflection $\mathrm{SS_E}$ constructed by the PP+PS=SS method:

$$\begin{aligned} |U_{SS_E}| &= \frac{|U_{PS_{E1}}|\,|U_{PS_{E2}}|}{|U_{PP_E}|} \\ &= \mathcal{G}_E\, S(\omega)\, e^{-k^I_{S,DR}\,l_{DR}\,-\,k^I_{S,RC}\,l_{RC}}, \end{aligned} \quad (9)$$

where the ratio $\mathcal{G}_E = \mathcal{G}_{PS1_E}\,\mathcal{G}_{PS2_E}/\mathcal{G}_{PP_E}$ is assumed to be independent of frequency. It should be noted that $|U_{SS_E}|$ in equation 9 does not represent the actual amplitude of the primary SS reflection. While the PP+PS=SS method reproduces the kinematics of shear-wave primaries, it cannot yield the true amplitudes without knowledge of the velocity model (Grechka and Tsvankin, 2002; Grechka and Dewangan, 2003). Although equation 9 can be used to obtain the effective S-wave attenuation coefficient by evaluating the slope of $\ln|U_{SS_E}|$, its application is hampered by the need to evaluate the source spectrum $S(\omega)$, which is often difficult to do in practice.

However, as shown below, $S(\omega)$ is eliminated in the estimation of the interval S-wave attenuation coefficient. The ray-theoretic frequency-domain amplitudes of the waves $\mathrm{PP_{O1}}$ and $\mathrm{PS_{O1}}$ (Figure 2) can be written as

$$\begin{aligned} |U_{PP_{O1}}| &= S(\omega)\,\mathcal{G}_{PP_{O1}}\, e^{-k^I_{P,O1}\,(l_{EI}\,+\,l_{IF})} \\ &= S(\omega)\,\mathcal{G}_{PP_{O1}}\, e^{-2\,k^I_{P,O1}\,l_{EI}}, \end{aligned} \quad (10)$$

$$|U_{PS_{O1}}| = S(\omega)\,\mathcal{G}_{PS_{O1}}\, e^{-k^I_{P,O1}\,l_{EI}}\, e^{-k^I_{S,O1}\,l_{ID}}, \quad (11)$$

where $k^I_{P,O1}$ and $k^I_{S,O1}$ are the average P-wave and S-wave group attenuation coefficients along the raypaths $\mathrm{PP_{O1}}$ and $\mathrm{PS_{O1}}$, respectively. Equations 10 and 11 can be combined to compute the attenuation of the constructed shear-wave $\mathrm{SS_{O1}}$ in the overburden:

$$|U_{SS_{O1}}| = \frac{|U_{PS_{O1}}|^2}{|U_{PP_{O1}}|} = \mathcal{G}_{O1}\, S(\omega)\, e^{-2\,k^I_{S,O1}\,l_{ID}}, \quad (12)$$

where $\mathcal{G}_{O1} = \mathcal{G}^2_{PS_{O1}}/\mathcal{G}_{PP_{O1}}$. Likewise, the attenuation coefficient for the overburden event $\mathrm{SS_{O2}}$ can be found from

$$|U_{SS_{O2}}| = \frac{|U_{PS_{O2}}|^2}{|U_{PP_{O2}}|} = \mathcal{G}_{O2}\, S(\omega)\, e^{-2\,k^I_{S,O2}\,l_{JC}}, \quad (13)$$

The problem is now reduced to the attenuation analysis of pure modes considered by Behura and Tsvankin (2009). Equations 9, 12 and 13 can be combined to compute the interval shear-wave attenuation in the target layer as follows:

$$\begin{aligned} |U_{SS_T}| &= \frac{|U_{SS_E}|^2}{|U_{SS_{O1}}|\,|U_{SS_{O2}}|} \\ &= \mathcal{G}_T\, e^{-2(\,k^I_{S,DR}\,l_{DR}\,+\,k^I_{S,RC}\,l_{RC})} \\ &\quad e^{2\,(k^I_{S,O1}\,l_{ID}\,+\,k^I_{S,O2}\,l_{JC})}, \end{aligned} \quad (14)$$

where $\mathcal{G}_T = \mathcal{G}^2_E/\,(\mathcal{G}_{O1}\,\mathcal{G}_{O2})$. Taking the logarithm of equation 14 yields:

$$\begin{aligned} \ln|U_{SS_T}| &= \ln\mathcal{G}_T\, -2(\,k^I_{S,DR}\,l_{DR}+\,k^I_{S,RC}\,l_{RC}) \\ &\quad +2\,(k^I_{S,O1}\,l_{ID}\,+\,k^I_{S,O2}\,l_{JC}). \end{aligned} \quad (15)$$

Since $k^I_{S,DR}\,l_{DR} = k^I_{S,IR}\,l_{IR} + k^I_{S,O1}\,l_{ID}$ and $k^I_{S,RC}\,l_{RC} = k^I_{S,RJ}\,l_{RJ} + k^I_{S,O2}\,l_{JC}$, equation 15 can be rewritten as

$$\begin{aligned} \ln|U_{SS_T}| &= \ln\mathcal{G}_T\, -2\,k^I_{S,IR}\,l_{IR}\, -2\,k^I_{S,RJ}\,l_{RJ} \\ &= \ln\mathcal{G}_T\, -2\,k^I_{S,T}\,(l_{IR}\,+\,l_{RJ}), \end{aligned} \quad (16)$$

where the coefficient $k^I_{S,T}$ represents the average group attenuation coefficient along the shear-wave raypath in the target layer.

Interval phase attenuation coefficient for a homogeneous target layer

If the target layer is heterogeneous, equation 16 provides only the offset-dependent average interval attenuation coefficient. Interpretation of attenuation measurements can be significantly simplified for horizontal, homogeneous layers with a horizontal symmetry plane. Then the length of the raypath in the target layer is given by $l_{IR} + l_{RJ} = V_g\,t_{SS_T}$, where V_g is the shear-wave group velocity along the ray IR (Figure 3), and t_{SS_T} is the interval shear-wave traveltime in the target layer. As a result, equation 16 reduces to

$$\ln|U_{SS_T}| \;=\; \ln\mathcal{G}_T\, -2\,k^I_{S,T}\,V_g\,t_{SS_T}. \quad (17)$$

Behura and Tsvankin (2009) show that equation 17 can be used to obtain the interval *phase* attenuation coefficient of P- or S-waves. According to their results, equation 17 can be rewritten as

$$\ln|U_{SS_T}| \;=\; \ln\mathcal{G}_T\, -2\,\omega\,\mathcal{A}_S\,t_{SS_T}, \quad (18)$$

where ω is the angular frequency and $\mathcal{A}_S = k^{I,Ph}/k^{R,Ph}$ is the S-wave phase attenuation coefficient (Zhu, 2006) for a zero inhomogeneity angle (the angle between the real and imaginary parts of the wave vector); $k^{I,Ph}$ and

$k^{R,Ph}$ are the magnitudes of the imaginary and real parts of the wave vector, respectively, for S-waves.

The shear-wave interval traveltime in the target layer (t_{SS_T}) is computed from equation 5 using the kinematic layer stripping. Hence, the slope of the logarithmic spectral ratio in equation 18 yields the phase attenuation coefficient for the phase angle corresponding to a given group direction (e.g., to the raypath IR in Figure 3). If the slope is constant, $\mathcal{A}_S$ and the quality factor $Q_S \approx 1/(2\,\mathcal{A}_S)$ are independent of frequency. If the slope varies with frequency, $\mathcal{A}_S$ has to be computed from the instantaneous slope, which yields a frequency-dependent attenuation coefficient and quality factor.

For VTI and orthorhombic media, the S-wave phase attenuation coefficient can be inverted for the attenuation-anisotropy parameters introduced by Zhu and Tsvankin (2006, 2007). The SV-wave phase attenuation coefficient in VTI media is approximately given by (Zhu and Tsvankin, 2006):

$$\mathcal{A}_{SV}(\theta) = \mathcal{A}_{S0}\,(1 + \sigma_Q\,\sin^2\theta\,\cos^2\theta), \qquad (19)$$

where $\mathcal{A}_{S0} \approx 1/(2Q_{S0})$ is the symmetry-direction SV attenuation coefficient and Q_{S0} is the vertical quality factor. The parameter σ_Q determines the variation of $\mathcal{A}_{SV}$ away from the symmetry direction and depends on the attenuation-anisotropy parameters ϵ_Q and δ_Q, as well as on the vertical velocities and quality factors P- and S-waves.

Whereas the phase attenuation coefficient is expressed as a function of the phase angle, our method computes $\mathcal{A}_{SV}$ for a certain source-receiver offset at the top of the target layer. Estimating the phase angle for a given source-receiver pair generally requires knowledge of the anisotropic velocity field in the interval of interest.

Synthetic example

The method was tested on synthetic multicomponent data from a horizontally stratified VTI model (Figure 4). The sources were placed on the top of the model, while the receivers were on the bottom of the water layer. Our method is applicable to this source-receiver geometry because it utilizes events with shared ray segments in the overburden.

Synthetic reflection data were generated using an anisotropic reflectivity code (Schmidt and Tango, 1986). PP and PS events from the top and bottom of the target were identified on the vertical and radial displacement components of the shot gather (Figure 5). Kinematic layer stripping of the shear-wave traveltimes produced the interval moveout in the third (target) layer shown in Figure 6. The layer-stripped interval traveltimes practically coincide with the exact values computed by ray tracing. It should be noted that the maximum offset for the constructed shear-wave in the target layer is limited

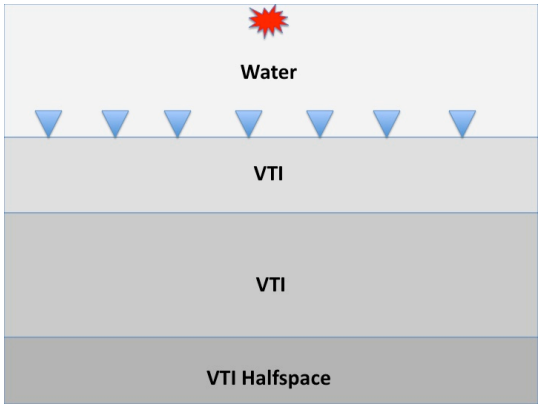

Figure 4. Synthetic model used to test the algorithm. The source is placed on the top of the model and the receivers are on the water bottom. The water is purely isotropic and elastic with the P-wave velocity $V_P = 1500$ m/s and thickness $d = 2000$ m. The other three layers have VTI symmetry for both velocity and attenuation. For the second layer, the vertical P- and S-wave velocities are $V_{P0} = 1600$ m/s and $V_{S0} = 800$ m/s, thickness $d = 600$ m, and velocity-anisotropy parameters are $\epsilon = 0.30$, and $\delta = 0.10$; the attenuation parameters are $Q_{P0} = 20$, $Q_{S0} = 50$, $\epsilon_Q = 0.30$, and $\delta_Q = 0.20$. In the third layer, $V_{P0} = 1700$ m/s, $V_{S0} = 900$ m/s, $d = 1000$ m, $\epsilon = 0.25$, $\delta = 0.10$, $Q_{P0} = 100$, $Q_{S0} = 20$, $\epsilon_Q = 0.20$, and $\delta_Q = 0.10$. The parameters of the bottom halfspace are $V_{P0} = 2500$ m/s, $V_{S0} = 1400$ m/s , $\epsilon = 0.30$, $\delta = 0.10$, $Q_{P0} = 50$, $Q_{S0} = 50$, $\epsilon_Q = 0.40$, and $\delta_Q = 0.30$.

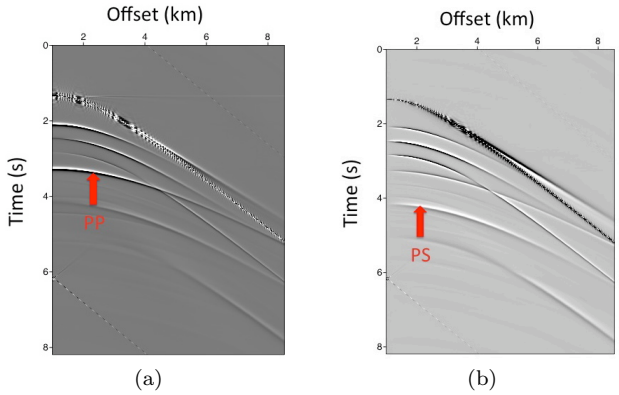

Figure 5. Vertical (a) and horizontal (b) displacement components of a shot gather for the model from Figure 4. The target PP and PS events are marked by the red arrows in (a) and (b), respectively.

by the critical angle for SP mode conversions, which is equal to 32°.

The input amplitudes were obtained by computing the vector sum of the radial and vertical displacement components. Frequency-domain amplitudes were found by windowing the arrivals and applying the Fourier transform. The target layer is horizontal, homogeneous,

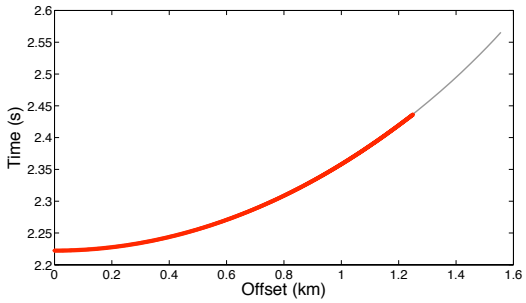

Figure 6. Interval shear-wave traveltime in the third layer (red stars) computed using the PP+PS=SS method and velocity-independent layer-stripping. The gray curve marks the exact traveltime.

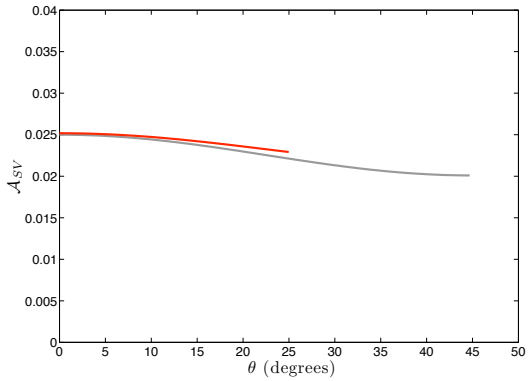

Figure 7. Estimated S-wave interval phase attenuation coefficient $\mathcal{A}_{SV}$ for the third layer (red line) as a function of the phase angle θ. The gray line marks the exact coefficient $\mathcal{A}_{SV}$.

and has a horizontal plane of symmetry (it is VTI). Therefore, the interval shear-wave phase attenuation coefficient in the target layer was computed from equation 18 using the algorithm discussed above. The SV-wave phase angles were obtained from the corresponding group angles using the known velocity function in the target layer. The parameters $\mathcal{A}_{S0} = 0.025$ and $\sigma_Q = -0.61$ were found by least-squares fitting of equation 19 to the estimated values of shear-wave phase attenuation coefficient $\mathcal{A}_{SV}$. The obtained parameter $\mathcal{A}_{S0}$ is close to its actual value (0.025), but there is a significant error in the parameter σ_Q (the actual value is -0.78) due to the limited range of phase angles for the reflected S-leg of the PS-wave. The exact and best-fit curves of the shear-wave phase attenuation coefficient $\mathcal{A}_{SV}$ are displayed in Figure 7.

Discussion

Despite the generally successful test results, the proposed method has several limitations. First, the range of phase angles for the constructed SS-wave is restricted due to two factors: the small amplitudes of PS-waves at near offsets and the critical angle for converted waves. Typical values for the critical angle are about 30°, which causes instability in the inversion for the attenuation-anisotropy parameter σ_Q. Estimation of σ_Q may be more accurate for hard rocks with a high V_S/V_P ratio, for which the critical angle for SP mode conversions is higher. However, the algorithm should provide tight constraints on the symmetry-direction coefficient $\mathcal{A}_{S0}$. Second, because the data are generated by a P-wave source, it is necessary to repeatedly apply the PP+PS=SS method to construct SS events, which could lead to error accumulation in the attenuation analysis. Third, the algorithm is supposed to operate with isolated reflection events. Amplitude distortions due to interference (e.g. with multiples) may hinder S-wave attenuation estimates.

To express $\mathcal{A}_{SV}$ as a function of the phase angle (equation 19), it is necessary to know the velocity function. However, as discussed by Behura and Tsvankin (2009), the difference between the phase and group angles for moderately anisotropic models does not substantially distort attenuation coefficients. It should be mentioned, however, that even computation of the group angle for a given source-receiver pair requires velocity information.

Conclusions

We extended the algorithm of Behura and Tsvankin (2009), originally introduced for pure modes, to the combination of PP- and PS-waves with the goal of estimating the shear-wave interval attenuation coefficient. Our technique involves repeated application of the PP+PS=SS method followed by velocity-independent layer stripping (VILS), for both traveltime and frequency-domain amplitudes. In the 2D implementation of the method discussed here, the vertical incidence plane has to be a plane of mirror symmetry in all layers including the target. VILS is designed for a laterally homogeneous (although possibly vertically heterogeneous) overburden with a horizontal symmetry plane in each layer. If this assumption is satisfied, our method does not require knowledge of the overburden velocity and attenuation parameters.

For heterogeneous target layers, the algorithm estimates the average S-wave interval group attenuation coefficient for a range of source-receiver offsets. If the target is horizontal, homogeneous, and has a horizontal symmetry plane, it is possible to obtain the interval phase attenuation coefficient for the constructed SS events.

Synthetic modeling for layered VTI media confirmed the accuracy of the method in estimating the interval SV-wave phase attenuation coefficient $\mathcal{A}_{SV}$. The range of phase angles for the constructed SS reflection is limited by the small amplitudes of PS-waves at near offsets and the critical angle for the reflected S-leg. The coefficient $\mathcal{A}_{SV}$ can be inverted for the symmetry-direction coefficient $\mathcal{A}_{S0}$ and, under favorable circumstances, for the attenuation-anisotropy parameter σ_Q.

The combination of the shear-wave attenuation coefficient with P-wave attenuation measurements can help detect the presence of fluids in a reservoir. The 3D version of our method can be applied to wide-azimuth data to evaluate the azimuthal variation of shear-wave attenuation, which is sensitive to fluid-filled natural fracture sets.

Acknowledgments

We are grateful to the members of the A(nisotropy)-Team of the Center for Wave Phenomena (CWP), Colorado School of Mines, for fruitful discussions. Support for this work was provided by the Consortium Project on Seismic Inverse Methods for Complex Structures at CWP and by the Research Partnership to Secure Energy for America (RPSEA).

References

Adam, L., 2008, Elastic and visco-elastic laboratory properties in carbonates: PhD thesis, Colorado School of Mines.

Batzle, M., R. Hofmann, and M. Prasad, 2005, Seismic attenuation: Observations and mechanisms: 75th Annual International Meeting, SEG, Expanded Abstracts, 1565–1568.

Behura, J., M. Batzle, R. Hofmann, and J. Dorgan, 2007, Heavy oils: Their shear story: Geophysics, **72**, no.5, E175–E183.

Behura, J. and I. Tsvankin, 2009, Estimation of interval anisotropic attenuation from reflection data: Geophysics, **74**, no.6, A69–74.

Chichinina, T., I. Obolentseva, L. Gilk, B. Bobrov, and G. Ronquillo-Jarillo, 2009, Attenuation anisotropy in the linear-slip model: Interpretation of physical modeling data: Geophysics, **74**, no.5, WB165–WB176.

De, G. S., D. F. Winterstein, and M. A. Meadows, 1994, Comparision of P- and S-wave velocities and Q's from VSP and sonic log data: Geophysics, **59**, 1512–1529.

Dewangan, P. and I. Tsvankin, 2006, Velocity-independent layer stripping of PP and PS reflection traveltimes: Geophysics, **71**, no.4, U59–U65.

Dvorkin, J. P. and G. Mavko, 2006, Modeling attenuation in reservoir and nonreservoir rock: The Leading Edge, **25**, 194–197.

Grechka, V. and P. Dewangan, 2003, Generation and processing of pseudo-shear-wave data: Theory and case study: Geophysics, **68**, 1807–1816.

Grechka, V. and I. Tsvankin, 2002, PP + PS = SS: Geophysics, **67**, 1961–1971.

Liu, E., M. Chapman, I. Varela, X. Li, J. H. Queen, and H. Lynn, 2007, Velocity and attenuation anisotropy: Implication of seismic fracture charecterizations: The Leading Edge, **26**, 1170–1174.

Schmidt, H. and G. Tango, 1986, Efficient global matrix approach to the computation of synthetic seismograms: Geophysical Journal of the Royal Astronomical Society, **84**, 331–359.

Zhu, Y., 2006, Seismic wave propagation in attenuative anisotropic media: PhD thesis, Colorado School of Mines.

Zhu, Y. and I. Tsvankin, 2006, Plane-wave propagation in attenuative transversely isotropic media: Geophysics, **71**, no.2, T17–T30.

———, 2007, Plane-wave attenuation anisotropy in orthorhombic media: Geophysics, **72**, no.1, D9–D19.

Zhu, Y., I. Tsvankin, and I. Vasconcelos, 2007, Effective attenuation anisotropy of thin-layered media: Geophysics, **72**, no.5, D93–D106.